Probing the Recognition Properties of the Antiparallel Coiled Coil Motif from PKN by Protein Grafting[†]

Yinyin Li, Harmeet Kaur, and Martha G. Oakley*

Department of Chemistry, Indiana University, 800 East Kirkwood Avenue, Bloomington, Indiana 47405-7102

Received September 12, 2008; Revised Manuscript Received November 4, 2008

ABSTRACT: Coiled coils have long been recognized as the major constituent of many fibrous proteins and also serve as oligomerization domains in a wide variety of proteins. More recently, it has become clear that the surfaces of two-stranded coiled coils are also involved in macromolecular recognition. Indeed, the helical hairpin or intramolecular antiparallel coiled coil (ACC) can serve as a protein or nucleic acid recognition motif. Protein kinase N (PKN) interacts with the small GTPase RhoA through ACC motifs. The crystal structure of RhoA with the N-terminal ACC motif (PKN-ACC1) is unusual in that these proteins interact through two distinct surfaces. Using the ACC domain of seryl tRNA synthetase (SRS-ACC) as a scaffold for protein grafting experiments, we show that RhoA interacts with only one face of PKN-ACC1. This result highlights the potential of the SRS-ACC scaffold for protein engineering applications and provides insight into the mechanism of RhoA-mediated signal transduction through PKN.

The coiled coil is a widespread structural motif consisting of two or more α-helices that twist around each other in a left-handed fashion (*3*−*7*). Coiled coil sequences are characterized by a heptad repeat of amino acids denoted **abcdefg** (*3*−*6*). The residues at the **a** and **d** positions are predominantly hydrophobic, with polar or charged residues generally occupying the remaining positions (*3*−*6*). During the past two decades, extensive studies have probed the factors that influence the stability and quaternary structure of natural and designed coiled coils (*3*−*6*). These studies have not only enhanced our understanding of the role of coiled coils in biology but have also greatly facilitated the design of coiled-coil proteins for applications including affinity purification, the preparation of materials with defined properties, and the inhibition of viral membrane fusion (*5, 8*−*13*).

The vast majority of coiled coils that have been studied align with their constituent helices in a parallel fashion (*3*−*6*). However, it has become increasingly clear that antiparallel coiled coils are much more prevalent than was initially thought (*14, 15*). One of the most common types of antiparallel coiled coils is the helical hairpin or antiparallel coiled coil (ACC[1]) motif, which consists of two helical strands connected through a short loop (*4, 14*). Instead of mediating protein oligomerization, these intramolecular, antiparallel coiled coils appear to be involved primarily in molecular recognition, interacting with other macromolecules along the coiled coil surface.[2]

The ACC is a versatile molecular recognition motif that can interact with proteins (*16*−*20*), RNA (*21*−*23*), or DNA (*24*). For example, the ACC domain of *Escherichia coli* (*E. coli*) seryl tRNA synthetase (SRS) engages in extensive interactions with the variable arm of seryl-tRNA (*21, 23, 25*−*27*), while ACC domains located at the *N*-terminus of protein kinase N (PKN) mediate protein−protein interactions with RhoA (*28*−*34*) (Figure 1A). In spite of the fact that the ACC domains from PKN and SRS interact with different classes of macromolecules, the overall structures of SRS-ACC and PKN-ACC1 are remarkably similar (Figure 1B). Indeed, a structural overlay of the two structures results in a root-mean-square deviation of approximately 1 Å for the alpha carbons. This observation suggests that the determinants of ACC structure are independent of its binding specificity. Thus, it stands to reason that the recognition properties of ACC domains may be modified simply by grafting the appropriate surface residues onto any ACC scaffold.

PKN, also known as protein kinase C-related kinase 1 (PRK1), was one of the first downstream effectors to be identified for RhoA, a small GTPase involved in the

[†] This work was supported by the National Institutes of Health (GM 57571).

* Corresponding author. E-mail: oakley@indiana.edu. Phone: (812) 855-4843. Fax: (812) 855-8300.

[1] Abbreviations: PKN, protein kinase N; PRK1, protein kinase C-related kinase 1; SRS, seryl tRNA synthetase; ACC, antiparallel coiled coil; HPC1, Hybrid Protein Contact 1; HPC2, Hybrid Protein Contact 2; SMC, structural maintenance of chromosomes; APP, avian pancreatic polypeptide; HIV, human immunodeficiency virus; PCR, polymerase chain reaction; SDS−PAGE, sodium dodecyl sulfate polyacrylamide gel electrophoresis; CD, circular dichroism; SPR, surface plasmon resonance; HPLC, high performance liquid chromatography; Ni-NTA, nickel-nitrilotriacetic acid; GTP, guanosine-5′-triphosphate; GDP, guanosine-5′-diphosphate; GTPγS, guanosine-5′-3-*O*-(thio)triphosphate; IPTG, isopropyl-β-D-thiogalactopyranoside; LB, Luria−Bertani; DTT, dithiothreitol; EDTA, ethylenediaminetetraacetic acid; HEPES, 4-(2-hydroxyethyl)piperazine-1-ethanesulfonic acid; PBS, phosphate-buffered saline; NHS, *N*-hydroxysuccinimide; EDC, 1-ethyl-3-(3-dimethylaminopropyl)carbodiimide hydrochloride; T_m, midpoint of the thermal unfolding transition; RU, response unit; K_d, dissociation constant; $[\theta]_{222}$, molar elipticity at 222 nm; OD_{600}, optical density at 600 nm.

[2] We note that long antiparallel coiled coils, like those found in the Rad50 and structural maintenance of chromosomes (SMC) proteins, can also mediate protein−protein interactions (*1, 2*). However, we use the term ACC here to refer only to the helical hairpin class of coiled coils.

10.1021/bi8017448 CCC: $40.75
Published on Web 12/02/2008

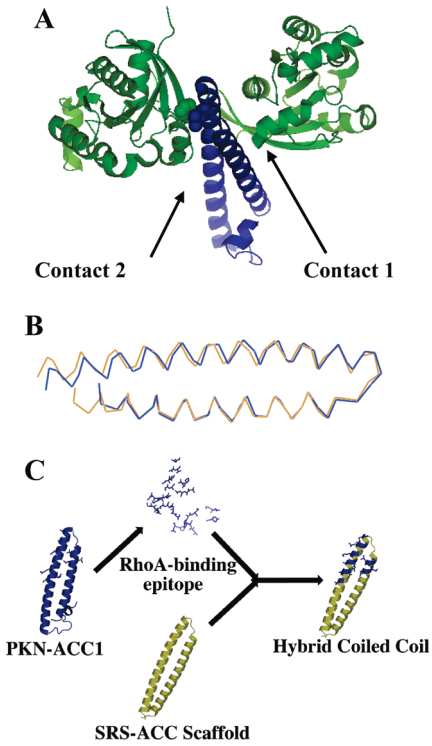

FIGURE 1: Design of hybrid coiled-coil proteins. (A) Two contact interfaces within PKN-ACC1·RhoA complex. Although PKN-ACC1 (blue) and RhoA (green) form a 1:1 complex in the crystal (*16*), there are two distinct interaction surfaces between them. Residues F39 of RhoA and L59 of PKN-ACC1 are highlighted (space-filled). (B) Structural overlay of PKN-ACC1 (blue) and SRS-ACC (yellow). (C) Protein grafting approach. The surface residues of SRS-ACC are partially substituted by the RhoA-binding epitope from PKN-ACC1. The figures were prepared using PyMOL (PKN-ACC1·RhoA from PDB: 1CXZ (*16*); SRS-ACC from the coordinates provided by Dr. Cusack (*71*)).

regulation of the cytoskeleton in response to external stimuli (*28, 29, 35*−*37*). This serine/threonine protein kinase has also been implicated in a range of additional cellular processes, including cell adhesion, apoptosis, meiotic maturation and embryonic development (*38*). The crystal structure of a 1:1 complex of PKN-ACC1 and RhoA has been solved (*16*). Surprisingly, two distinct interaction surfaces were identified, which were designated Contact 1 and Contact 2 (*16*) (Figure 1A). The two binding interfaces involve opposite faces of PKN-ACC1 and nonoverlapping sites on RhoA. It has generally been presumed that one of these interactions is an artifact of crystal packing or of the high protein concentration used for crystallization.

Contact 1, with a surface area of 2080 Å^2, is made up of a hydrogen bond and salt bridge network typical of protein−protein interaction surfaces (*16*). This binding interface is formed from the lower (**b**, **e**) face of PKN-ACC1 (Figure 2B) and from the region including α1, α5 and *β*2/*β*3 of RhoA (Figure 1A). The conformation of this region of RhoA does not change significantly in response to GTP hydrolysis. In contrast, Contact 2 is smaller, at 1640 Å^2, and includes the "switch" regions of RhoA that undergo large conformational changes upon GTP hydrolysis (*16, 39, 40*). These "switch" regions interact along the upper (**c, g**) face of the PKN-ACC1 motif (Figure 2B). Arguments in support of the physiological relevance of each interface have been put forward in the literature (*16, 30, 34, 41, 42*), but this issue remains unresolved.

To address this question, we employed a protein grafting approach. Protein grafting is an emerging field to impart a scaffold protein with designed binding specificity (*43*−*54*). We used the SRS-ACC as a scaffold, as it is an autonomously folded domain that is readily overexpressed in *E. coli* (*55*). We separately grafted the PKN residues involved in Contact 1 and Contact 2 into the SRS-ACC scaffold (Figure 1C). The structure and binding specificity of the two engineered ACCs were then monitored to probe both the versatility of the ACC as a recognition domain and the potential roles of the proposed RhoA binding sites for PKN function.

MATERIALS AND METHODS

Plasmid Construction. To facilitate bacterial expression, protein genes were optimized using high frequency codons according to the *E. coli* codon usage table (*56*). The genes encoding Hybrid Protein Contact 1 (HPC1) and Hybrid Protein Contact 2 (HPC2) were constructed by single step recursive PCR (*57*−*60*). In general, long oligonucleotides were 80 bases in length with an overlapping stretch of 20 nucleotides. Short oligonucleotides were approximately 20 nucleotides long with melting temperatures around 50 °C. Due to the larger size of its gene (∼450 bp), PKN-ACC1 (7−155) was synthesized using asymmetric PCR (*60, 61*). In addition, one 32-cycle PCR reaction using two short oligonucleotides annealing to the terminal regions of the gene was used to amplify the final product. The SRS-ACC (25−104) gene was amplified from pSRS-82 (*55*). Each of the above gene fragments was subcloned between the *Nde*I and *Eco*RI or *Bam*HI sites of pET-28a+.

RhoA-pGEX-2T was a kind gift from Dr. Andrew Feig. To decrease the GTP hydrolysis activity of RhoA, a G14V mutation was introduced; this mutation greatly reduces the rate of GTP hydrolysis with no effect on RhoA's PKN binding activity (*28, 29, 62*). For simplicity, this mutant protein will be referred to as RhoA in this paper. The mutant proteins HPC2-L57K, PKN-ACC1-L59K and RhoA-F39A were made by site directed mutagenesis using the Quikchange method (Qiagen) or by an overlapping extension PCR method (*63*). Protein and oligonucleotide sequences are listed in the Supporting Information (Tables S1−S3). All sequences were confirmed by DNA sequencing (*64*).

Protein Expression and Purification. Recombinant coiled-coil proteins were expressed in BL21 (DE3) cells using the T7 system (*65*). A 700 mL culture was grown in Luria−Bertani (LB) broth with kanamycin (10−50 *μ*g/mL) at 37 °C to an optical density at 600 nm (OD_{600}) of 0.4−0.7. Protein overexpression was induced by addition of isopropyl-*β*-D-thiogalactopyranoside (IPTG) to a final concentration of 0.5 mM. After an additional incubation of 3−5 h, cells were harvested by centrifugation and lysed by sonication in 20 mL of lysis buffer (50 mM sodium phosphate, 300 mM NaCl, 10 mM imidazole, pH 8.0). After centrifugation to remove cellular debris, the cell lysates were mixed with nickel-nitrilotriacetic acid (Ni-NTA) agarose beads (Qiagen; 2 mL) and washed with 50 mL of wash buffer (50 mM sodium phosphate, 300 mM NaCl, 20 mM imidazole, pH 8.0). The bound proteins were eluted in 20 mL of elution buffer (50 mM sodium phosphate, 300 mM NaCl, 250 mM imidazole, pH 8.0). The eluted proteins were further purified through a C18 reverse phase column (Grace Vydac) on a

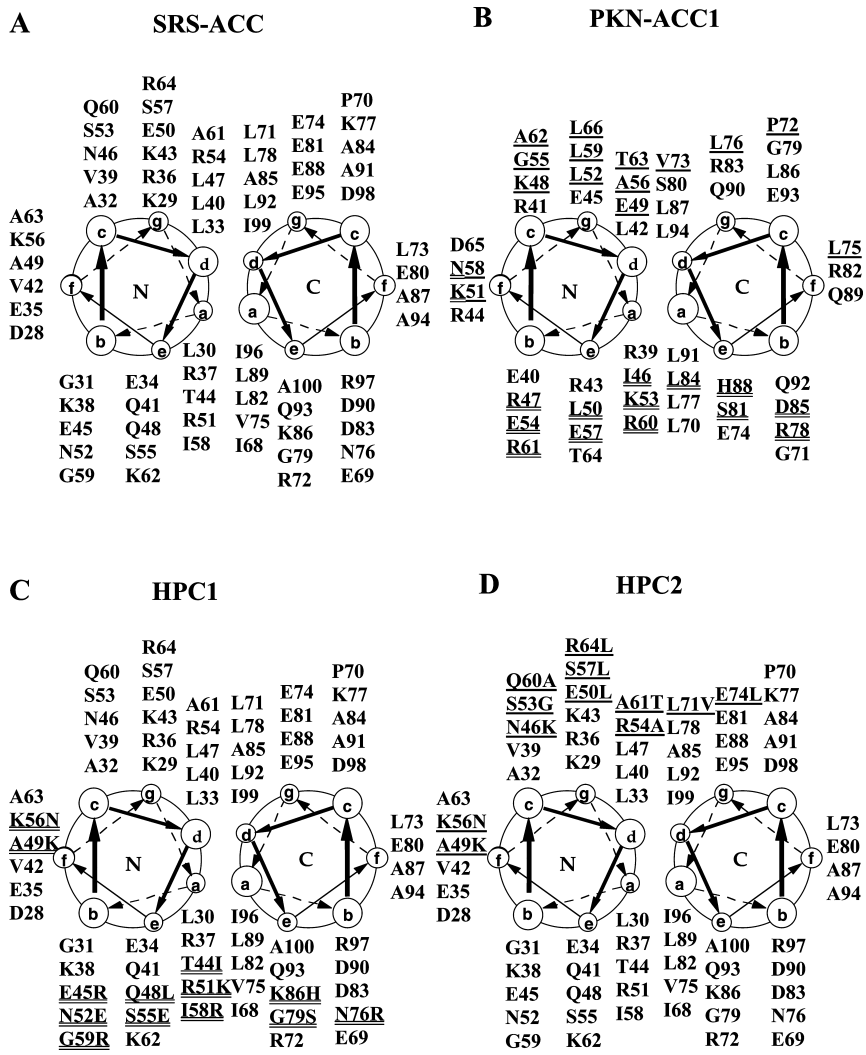

FIGURE 2: Helical wheel representations of ACC proteins. (A) SRS-ACC. (B) PKN-ACC1. Residues contacting RhoA are highlighted with double (Contact 1) or single (Contact 2) underscores. (C) HPC1. SRS-ACC residues that have been replaced by the corresponding residues in PKN-ACC1 are doubly underscored. (D) HPC2. SRS-ACC residues that have been replaced by PKN-ACC1 residues are underscored.

Prostar 210/215 high performance liquid chromatography (HPLC) system (Varian) with a linear acetonitrile/H_2O gradient (10%−70%). The collected fractions were dried by lyophilization (Freezeone 4.5, Labconco) for long-term storage. The molecular masses of coiled-coil proteins were verified by matrix assisted laser desorption ionization time-of-flight mass spectrometry (MALDI-TOF-MS).

For the expression of RhoA, a 700 mL LB culture with ampicillin (100 μg/mL) was grown to an OD_{600} of 0.4−0.7 at 37 °C. The culture was then moved to 25 °C and IPTG was added to a final concentration of 0.1 mM. After 2−3 h, the cells were harvested by centrifugation and lysed by sonication in 15 mL phosphate-buffered saline (PBS) buffer (10.1 mM sodium phosphate, 1.76 mM potassium phosphate, 137 mM NaCl, 2.68 mM KCl, pH 7.4) with 1 mM dithiothreitol (DTT). After centrifugation to remove cellular debris, the lysate was incubated with 1 mL of glutathione-sepharose (Amersham) at 4 °C for 1.5 h, and washed with PBS buffer (3 × 12 mL). Finally, the bound protein was eluted with reduced glutathione (10 mM, 4 × 1 mL) in PBS buffer (pH 8.0). All proteins were at least 90% pure as judged by sodium dodecyl sulfate polyacrylamide gel electrophoresis (SDS−PAGE).

Circular Dichroism (CD) Spectroscopy. CD spectra were obtained on a Jasco J-715 spectropolarimeter. First, proteins were dialyzed into PBS buffer. Concentrations were obtained using the method of Edelhoch (*66*). The wavelength dependence of molar elipticity [θ] was monitored in 1 nm increments with a 4 s response time at 4 °C. Thermal stability was assessed by the temperature dependence of $[\theta]_{222}$ from 4 to 90 °C (2 °C increments, 90 s equilibration time). Helical content was calculated by the method of Chen (*67*). The T_m of each thermal unfolding transition is estimated from the maximum of the first derivative curve.

Sedimentation Equilibrium Assays. Apparent molecular masses in solution were determined by equilibrium sedimentation on a Beckman Optima XL-1 at 4 °C. Samples were dialyzed against PBS buffer for at least 12 h. Data were collected at two different wavelengths and two different rotor speeds using an An-60 Ti rotor (Beckman). At every protein concentration, data from both rotor speeds were globally fitted to an ideal single species model of absorbance against radial distance with manufacturer supplied software (Origin). Partial molar volumes and solvent density were calculated by the method of Laue et al. (*68*).

Surface Plasmon Resonance (SPR). SPR assays were carried out on a Biacore 3000 instrument. All channels on a Ni-NTA chip (Biacore) were first cleaned with cleaning buffer (10 mM 4-(2-hydroxyethyl)piperazine-1-ethanesulfonic acid (HEPES), 150 mM NaCl, 300 mM ethylenediaminetetraacetic acid (EDTA), pH 8.2) at 20 μL/min. The channels were then equilibrated with a $NiCl_2$ solution (60 μL, 0.5 mM; 20 μL/min) to activate the surface. His-tagged protein (1 μM) in running buffer (10 mM HEPES, 150 mM NaCl, 10 mM $MgCl_2$, pH 7.4) was immobilized in the sampling channel by injection at 5 μL/min until a response of 1000−3000 RU was obtained. Because immobilized His-tagged protein dissociated at room temperature, disrupting the baseline, a temperature of 4 °C was used for all experiments, resulting in a stable baseline. The control channel signal was subtracted from the sample channel signal before plotting. RhoA was loaded with guanosine-5′-3-*O*-(thio)triphosphate (GTPγS) or guanosine-5′-diphosphate (GDP) by incubating with a 10-fold molar excess of nucleotide at room temperature for 30 min in nucleotide loading buffer (50 mM HEPES, 5 mM EDTA, 2 mM DTT, pH 7.6). The loading reaction was quenched via the addition of $MgCl_2$ (1 M stock) to a final concentration of 10 mM and placing on ice. The nucleotide-loaded RhoA was exchanged into running buffer with a PD-10 sized exclusion column (Amersham). Nucleotide-loaded RhoA proteins (1 μM; 40 μL) were injected at 20 μL/min to study the binding activity.

Quantitative equilibrium SPR was performed using a CM5 chip (Biacore). Coiled-coil proteins were covalently attached to the CM5 chip via amine coupling and remained stably attached to the chip after multiple regeneration cycles. To immobilize the proteins on the chip surface, the channel was first activated by injecting a 1:1 mixture of 100 mM *N*-hydroxysuccinimide (NHS) and 400 mM 1-ethyl-3-(3-dimethylaminopropyl)carbodiimide hydrochloride (EDC) at 5 μL/min. The coiled-coil protein (1 μM) was then injected in immobilization buffer (10 mM sodium acetate, pH 4.0 (HPC2) or 4.5 (PKN-ACC1)) at 5 μL/min until a response of 600−1000 RU was reached. Unreacted NHS ester was blocked by injection of 30 μL of 1 M ethanolamine (pH 8.5) at 5 μL/min. The blank channel was prepared in a similar fashion minus the injection of the coiled-coil proteins. To obtain a dissociation constant, nucleotide-loaded RhoA (200 μL; 0.1−8 μM) was injected at 10 μL/min until the binding surface was saturated with protein. Between cycles, regeneration of the binding surface was achieved by injecting 30 μL of regeneration buffer (6 M urea, pH 9.0) at 5 μL/min. The equilibrium binding assays were performed in triplicate. The data for each assay were regression fitted to a Langmuir model using Sigmaplot. The equation used is as follows: $R_{eq} = R_{max}C/(K_d + C)$, where R_{eq} is the steady state binding response, C is the concentration of nucleotide-loaded RhoA, R_{max} is the total surface binding capacity, and K_d is the dissociation constant. Reported dissociation constants are the average of three trials; the reported error is the standard deviation for the three repeated measurements.

To test further the effect of exchanging the ligand and analytes, 8.4 μM GTPγS -RhoA was diluted 1:10 into immobilization buffer (10 mM sodium acetate, pH 4.5) and then flowed over the CM5 chip activated as described above. RhoA was immobilized to approximately 1500 RU. Then coiled-coil proteins (40 μL; 1 μM) were injected at 20 μL/min to monitor binding.

RESULTS

Design of Hybrid ACC Proteins. The structural alignment of PKN-ACC1 and SRS-ACC is shown in Figure 1B. PKN-ACC1 residues involved in RhoA-binding were identified from the crystal structure (*16*) (Figure 2B). Both RhoA-binding epitopes involve residues near, but not including, the loop region of PKN-ACC1. Although there are discernible differences in the conformations of PKN-ACC1 and SRS-ACC in the loop region and in the N- and C-termini of the coiled coils, these regions of PKN-ACC1 are not involved in RhoA binding. In contrast, there is excellent agreement in the C_α positions of the two proteins in the region of PKN-ACC1 that mediates RhoA binding. Thus, it was a straightforward matter to identify the residues in the SRS-ACC to be replaced with PKN-ACC1 residues that constitute the RhoA-binding epitopes.

Both Contact 1 and Contact 2 have 15 residues that participate in the interaction with RhoA (Figure 2B), most of which are located on the surface of PKN-ACC1. These two sets of residues were separately grafted onto the SRS-ACC scaffold, yielding Hybrid Protein Contact 1 (HPC1) (Figure 2C) and Hybrid Protein Contact 2 (HPC2) (Figure 2D). HPC1 differs at 13 residues from the original SRS-ACC scaffold, including three residues at **a** positions (Figure 2C). Similarly, in HPC2, 12 SRS-ACC residues were replaced with the appropriate PKN residues, including three residues in **d** positions (Figure 2D). In HPC2, L47 was left unchanged because the L47E mutation rendered the protein insoluble (data not shown).

For use as a positive control, we attempted to express and purify two different truncated forms of PKN that contain the ACC1 motif. The shorter construct, containing residues 26−107, includes the coiled-coil region in the PKN-ACC1·RhoA cocrystal structure (*16*) along with short extensions at both the N- and C-termini. This protein was poorly expressed, suggesting that it is unfolded in the absence of N- and C-terminal extensions that were used for crystallization. We therefore used the larger version of the ACC1 domain containing residues 7−155 (*62*) for these studies.

Structural Characterization of HPC1 and HPC2. To investigate the effect of introducing a relatively large number of mutations into SRS-ACC on its secondary structure, the hybrid proteins were analyzed via circular dichroism (CD) (Figure 3). The CD spectra for SRS-ACC, HPC1 and HPC2 all exhibit characteristic minima at 208 and 222 nm, and the extent of the signal at 222 nm indicates that these proteins are highly helical (Figure 3A). These data suggest that the substitutions introduced have little or no effect on the helical structure of SRS-ACC. HPC2 and SRS-ACC also have similar stabilities to thermal denaturation (Figure 3B). HPC1 is more stable to thermal denaturation than is SRS-ACC, possibly due to the substitution of hydrophilic core residue (T44) from SRS with an isoleucine in HPC1 (Figure 3B).

In contrast, PKN-ACC1 (7−155) is only 18% helical as judged from its CD spectrum (Figure 3A), a value far lower than 40% helicity that was calculated from the crystal structure of the PKN-ACC1·RhoA complex (*16*). This

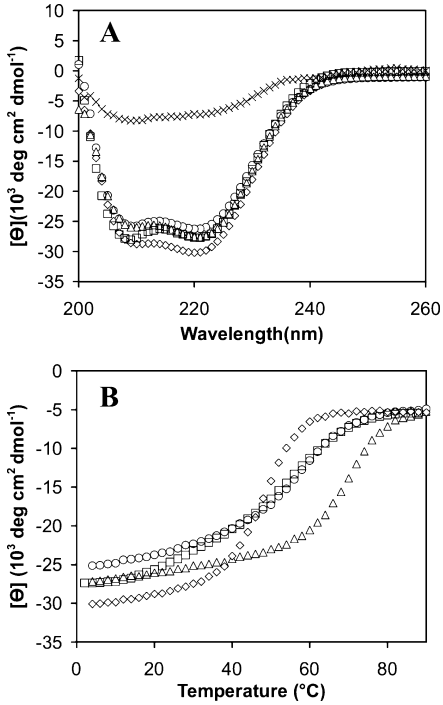

FIGURE 3: (A) Circular dichroism (CD) spectra of coiled-coil proteins at 4 °C in PBS buffer. The minima at 222 and 208 nm indicate that the designed proteins are highly helical. The values for $[\theta]_{222}$ indicate that HPC1 (△) is ca. 75% helical, HPC2 (○) is ca. 71% helical, SRS-ACC (◇) is ca. 83% helical, HPC2-L57K (□) is ca. 76% helical and PKN-ACC1 (×) is ca. 18% helical under these conditions. (B) Temperature dependence of the CD signal at 222 nm. HPC1 (△) = 70 °C; HPC2 (○) = 56 °C; SRS-ACC (◇) = 50 °C; HPC2-L57K (□) = 54 °C.

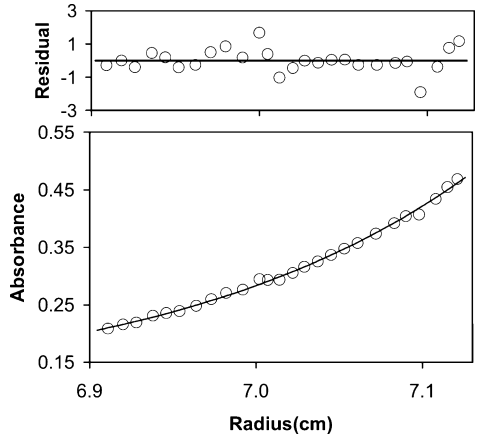

FIGURE 4: Representative analytical ultracentrifuge sedimentation data for HPC2 (4 °C, 7 μM, PBS buffer, pH 7.4, 23 krpm). Data from two different rotor speeds were globally fitted to an ideal single species model. The random residual distribution indicates the data fit well with an ideal single species model.

observation suggests that PKN-ACC1 is partially unfolded in the absence of its binding partner, RhoA.

Sedimentation equilibrium experiments were performed in order to probe the oligomerization properties of the hybrid coiled coils in solution. SRS-ACC is a monomer in solution (*55*). Similarly, our data suggest that the hybrid coiled-coil proteins are monomers under the conditions tested (Figure 4, Table 1). Although HPC2 showed slight aggregation at concentrations above 15 μM (Table 1), both proteins are monomeric even at concentrations greater than those used for RhoA binding studies (1 μM) (Table 1). In summary,

Table 1: Molecular Weight Determination by Sedimentation Equilibrium Ultracentrifugation

protein (rotor speed)	concn (μM)	M_r/M_r(calc)[a]
HPC1 (38 krpm, 33 krpm)	85	1.10
	20	1.10
HPC2 (28 krpm, 23 krpm)	15	1.28
	7	1.02

[a] Calculated mass for a single species.

the hybrid coiled-coil proteins are similar to SRS-ACC with respect to both overall structure and hydrodynamic properties.

Binding of the HPC Proteins to RhoA. We tested the RhoA binding activity of the hybrid coiled-coil proteins using surface plasmon resonance (SPR). The coiled-coil proteins were immobilized on a Ni-NTA chip via their His-tags. Following immobilization, GTPγS-RhoA was allowed to flow through the coiled-coil modified surface. GTPγS-RhoA clearly bound to both PKN-ACC1- and HPC2- modified surfaces (Figure 5A). In contrast, no binding interaction was detected for GTPγS-RhoA with HPC1- or SRS-ACC-modified surfaces. A slight negative response was observed due to nonspecific binding within the reference channel (Figure 5A).

To ensure that the results were not affected by the attachment of the coiled-coil proteins to the surface, GTPγS-RhoA was immobilized to the surface and the coiled-coil proteins were allowed to flow through (Figure 5B). Although lower response levels were observed due to the low molecular weights of the coiled-coil proteins relative to that of RhoA, the binding results were unaffected. Thus, HPC2 and PKN-ACC1 bind GTPγS -RhoA, while HPC1 and SRS-ACC do not.

Previous studies have shown that PKN-ACC1 has a higher binding affinity for GTP-RhoA than for GDP-RhoA (*30, 33*), and this binding preference is likely to be important for the ability of RhoA to control PKN activity (*28, 29*). To determine whether RhoA binding by HPC2 is sensitive to GTP hydrolysis, equilibrium SPR experiments were performed to obtain quantitative binding data for GTPγS-RhoA and GDP-RhoA. The dissociation constant (K_d) of PKN-ACC1 for GTPγS -RhoA (0.53 ± 0.03 μM) is half that observed for GDP-RhoA (0.98 ± 0.06 μM) (Figure 6A, Table 2), consistent with the previously observed increase in affinity for GTPγS-RhoA (*30, 33*). Similarly, HPC2 also shows a 2-fold increase in the binding affinity for GTPγS -RhoA (K_d = 1.7 ± 0.1 μM) relative to GDP-RhoA (K_d = 3.9 ± 1.1 μM) (Figure 6B, Table 2). Thus, the hybrid coiled coil, HPC2, shows the same modest preference for GTP-RhoA as does PKN-ACC1.

Finally, we used mutagenesis to probe the similarity between the RhoA-PKN Contact 2 and RhoA-HPC2 interfaces. The RhoA mutant F39A has been shown previously to be deficient in PKN-mediated signal transduction (*69*). As this mutation occurs in the Contact 2 interface with PKN, we assayed this mutant for binding to PKN-ACC1 and HPC2 by SPR. We detected no interaction between RhoA-F39A and PKN-ACC1 (Figure 5C), consistent with previous reports for intact PKN (*69*). Similarly, we detected no binding interaction between RhoA-F39A and HPC2, suggesting that

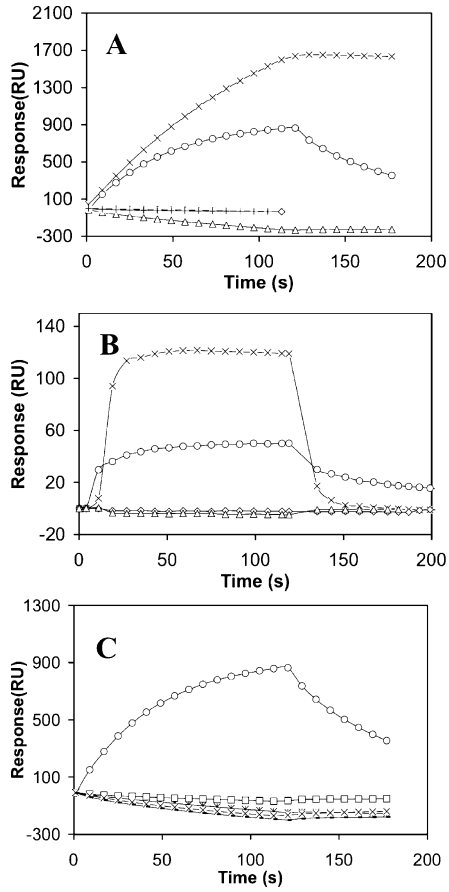

FIGURE 5: SPR sensorgrams providing a qualitative assessment of RhoA binding by coiled-coil proteins or their mutants. (A) Coiled-coil proteins were immobilized on Ni-NTA chip. GTPγS loaded RhoA was flowed through the channel. PKN-ACC1 ($\times$); HPC2 ($\bigcirc$); HPC1 ($\triangle$); SRS-ACC ($\diamond$); GST ($+$) was used as a control with HPC2. (B) GTPγS-RhoA was immobilized on a CM5 chip by amine coupling. Coiled-coil proteins were flowed through as analytes. PKN-ACC1 ($\times$); HPC2 ($\bigcirc$); HPC1 ($\triangle$); SRS-ACC ($\diamond$). (C) Coiled-coil proteins or their mutants were immobilized on Ni-NTA chip. GTPγS loaded RhoA or its mutant RhoA-F39A was flowed through the channel. HPC2-L57K/RhoA ($\square$); HPC2/RhoA-F39A ($*$); PKN-ACC1/RhoA-F39A ($\times$); PKN-ACC1-L59K/RhoA ($-$); HPC2/ RhoA ($\bigcirc$).

the hybrid coiled coil also interacts with the switch regions of RhoA (Figure 5C). In addition, we engineered a Contact 2 mutation into PKN and HPC2, substituting a Lys for a Leu residue (PKN-ACC1-L59K, HPC2-L57K). L59 occurs in the middle of a surface hydrophobic patch in the PKN-ACC1 and interacts directly with F39 in the PKN-ACC1·RhoA complex (*16*) (Figure 1A). This single point mutation is sufficient to eliminate detectable RhoA binding for both PKN-ACC1 and HPC2, confirming the importance of the **c**, **g** face of both coiled coils in RhoA binding. Importantly, the helical content and thermal stability of HPC2-L57K are indistinguishable from those of HPC2, suggesting that the coiled-coil structure is not affected by this mutation (Figure 3A, Figure 3B). Similarly, RhoA-F39A retains activity toward other effector proteins, suggesting that the structure of this mutant is not significantly compromised (*69*). Thus, these data demonstrate that HPC2 binds RhoA in a similar fashion as does PKN-ACC1.

DISCUSSION

There has been disagreement in the literature as to which of the two interaction modes observed in the crystal structure

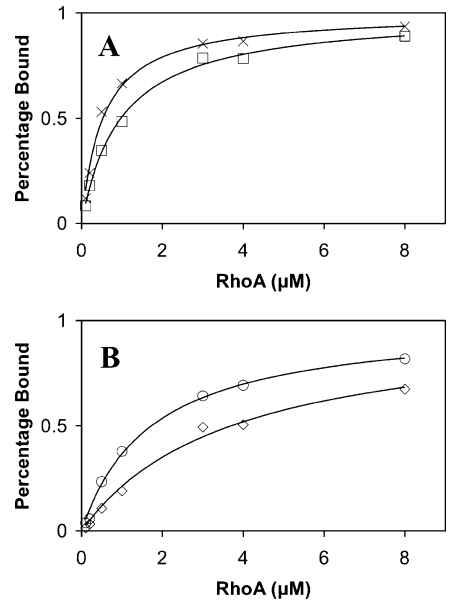

FIGURE 6: Concentration-dependence of equilibrium SPR signals for GTPγS- or GDP-RhoA binding with PKN-ACC1 (A) and HPC2 (B). PKN-ACC1 or HPC2 was amine coupled to a CM5 chip. Various concentrations (0.1, 0.2, 0.5, 1, 3, 4, 8 μM) of GTPγS- or GDP-RhoA were flowed through the channels until equilibrium was reached. The control channel signals were subtracted from the sample channel signals before plotting. Data are plotted as the percentage of the maximal response for comparison. PKN-ACC1/GTPγS-RhoA ($\times$); PKN-ACC1/GDP-RhoA ($\square$); HPC2/GTPγS-RhoA ($\bigcirc$); HPC2/GDP-RhoA ($\diamond$).

Table 2: K_d for GTPγS/GDP RhoA with PKN-ACC1 and HPC2

	K_d (μM)	
	GTPγS-RhoA	GDP-RhoA
PKN-ACC1	0.53 ± 0.03	0.98 ± 0.06
HPC2	1.7 ± 0.1	3.9 ± 1.1

of the PKN-ACC1·RhoA complex is physiologically relevant (*16, 30, 34, 41, 42*). It was initially proposed that Contact 1 is the physiologically relevant interface because it involves extensive H-bonding and Coulombic interactions and has larger buried surface area than does Contact 2 (*16*). On the other hand, the RhoA residues involved in Contact 2 correspond to those involved in the interaction between a variety Rho-type GTPases with their effector and regulatory partners (*41, 42*). Moreover, the Contact 2 interaction is more likely to explain the GTP dependence of the PKN·RhoA interaction. This region of RhoA, unlike the region involved in Contact 1, undergoes large conformational changes upon GTP hydrolysis (*16*). These observations suggest that the interaction seen in Contact 2 is a more likely candidate for RhoA-mediated signal transduction.

We used a protein grafting approach to distinguish between these two binding sites, introducing each site separately into an SRS-ACC scaffold. Our results strongly support the view that the Contact 2 interaction is the physiologically relevant one, while the Contact 1 interaction is an artifact. At micromolar concentrations, we detect no interaction between HPC1 and RhoA. In contrast, HPC2 binds to RhoA with a K_d only 3-fold higher than that of PKN-ACC1. In addition, HPC2 has the same modest preference for binding to the GTP-bound form of RhoA as does PKN-ACC1. Finally, point mutations at Contact 2 in either RhoA or PKN/HPC2 completely abolish RhoA-binding by both HPC2 and PKN-

ACC1. These results demonstrate that the PKN residues forming Contact 2 are both necessary and sufficient for binding to RhoA.

PKN contains three predicted ACC motifs in its N-terminal domain (*38*). Although ACC3 shows no detectable binding affinity for RhoA, ACC2 does bind, albeit with markedly lower affinity than does ACC1 (*30, 31, 33*). A construct containing both ACC1 and ACC2 binds to RhoA with approximately 2−3 fold higher affinity than does ACC1 (*31, 34*). To explain these observations, two models have been proposed in which both binding surfaces of RhoA interact with a PKN ACC (*30, 34*). Our results support the model of Ahamadian and colleagues, which suggests that RhoA first recognizes the high-affinity PKN-ACC1 motif through the Contact 2 surface and then uses its Contact 1 surface to bind PKN-ACC2 in a subsequent step (*30*).

In addition to containing two potential sites for interaction with RhoA, PKN-ACC1 is partially unfolded in solution, making it difficult to evaluate the structural consequences of mutations that affect RhoA binding. In contrast, SRS-ACC is well behaved and provides a robust scaffold for these protein grafting experiments. The replacement of 13 or 12 SRS-ACC residues in HPC1 and HPC2, respectively, compromised neither the structure nor the stability of the scaffold, even though three interior **a** or **d** residues were replaced in each case. However, the ACC scaffold did not tolerate substitution of L47 with Glu at a **d** position, suggesting that destabilizing mutations in the coiled coil interior are not accommodated as easily as surface mutations.

Schepartz and co-workers have demonstrated the power of protein grafting using the 31-residue avian pancreatic protein (aPP) as a scaffold. This small, versatile scaffold stabilizes molecular recognition motifs composed of a single α- or polyproline helix and has been used to recognize both DNA and protein ligands (*43*−*49*). In some cases, simply grafting the recognition epitope on the surface of aPP was sufficient to provide miniature proteins capable of high affinity and specific binding (*43*−*45*). In other cases, an additional molecular evolution step using phage display was required to afford a stable, specific miniprotein (*46*−*49*). Because of the small size of aPP, the use of this scaffold has been restricted to targeting ligands that interacts with a single α- or polyproline helix.

The parallel, homodimeric coiled coil from GCN4 has been used to target more extensive protein−protein interaction surfaces. Sia and Kim grafted a discontinuous 19-residue epitope from the HIV C-peptide on to the surface of GCN4 (*51*). This hybrid peptide was linked via a disulfide bond to GCN4. The resulting covalent heterodimer exhibited potent antiviral activity without further optimization and was more structured and therefore more stable to proteolytic digestion than was the C-peptide alone. Similarly, Serrano and co-workers grafted eight residues from two antiparallel helices of interleukin-4 on to the surface of GCN4 (*52*). This hybrid homodimer, which also required a disulfide linkage for stability, bound the target receptor with micromolar affinity.

These experiments using GCN4 suggest that coiled coils provide a good scaffold for protein grafting experiments. However, both of these hybrid proteins required the addition of an interhelical disulfide bond for stability. In contrast, both of our engineered SRS-ACC proteins maintain the structure and stability of the protein scaffold without the addition of further elements for stability. Thus, the SRS-ACC may have broader applicability for protein engineering efforts than previously used coiled coil homodimers.

In conclusion, we have shown that a hybrid coiled coil containing Contact 2 of PKN-ACC1 binds to RhoA in a fashion similar to that of PKN-ACC1. These results highlight both the versatility of the ACC as a molecular recognition motif and the potential of the SRS-ACC scaffold for protein engineering efforts. In addition, as this hybrid RhoA-binding ACC is stable and well behaved in solution, it may serve as a useful inhibitor in the study of RhoA-mediated signaling. Indeed, coiled coils and helical bundles are also involved in the recognition of other Rho-family GTPases and their binding partners (*41*), suggesting that similar hybrid proteins may be more broadly applied to the study of the fundamental processes these GTPases regulate (*37, 70*).

ACKNOWLEDGMENT

The authors thank Dr. Andrew Feig for sharing the plasmid RhoA-pGEX-2T. The authors also acknowledge Dr. Todd Stone for assistance with the biophysical characterization experiments, Chris Weitzel and Vince Waldman for careful reading of this manuscript.

NOTE ADDED AFTER ASAP PUBLICATION

There were errors in Figures 3−6 in the version published ASAP December 2, 2008; the corrected version was reposted December 16, 2008.

SUPPORTING INFORMATION AVAILABLE

The sequences of all proteins and oligonucleotides used for these experiments, and additional analytical ultracentrifuge sedimentation data for HPC2 and HPC1. This material is available free of charge via the Internet at http://pubs.acs.org.

REFERENCES

1. Sergeant, J., Taylor, E., Palecek, J., Fousteri, M., Andrews, E. A., Sweeney, S., Shinagawa, H., Watts, F. Z., and Lehmann, A. R. (2005) Composition and architecture of the Schizosaccharomyces pombe Rad18 (Smc5−6) complex. *Mol. Cell. Biol. 25*, 172–184.
2. Hopfner, K. P., Karcher, A., Craig, L., Woo, T. T., Carney, J. P., and Tainer, J. A. (2001) Structural biochemistry and interaction architecture of the DNA double-strand break repair Mre11 nuclease and Rad50-ATPase. *Cell 105*, 473–485.
3. Lupas, A. (1996) Coiled coils: new structures and new functions. *Trends Biochem. Sci. 21*, 375–382.
4. Lupas, A. N., and Gruber, M. (2005) The structure of α-helical coiled coils. *Adv. Protein Chem. 70*, 37–78.
5. Woolfson, D. N. (2005) The design of coiled-coil structures and assemblies. *Adv. Protein Chem. 70*, 79–112.
6. Parry, D. A., Fraser, R. D., and Squire, J. M. (2008) Fifty years of coiled-coils and α-helical bundles: A close relationship between sequence and structure. *J. Struct. Biol. 163*, 258–269.
7. Burkhard, P., Stetefeld, J., and Strelkov, S. V. (2001) Coiled coils: a highly versatile protein folding motif. *Trends. Cell Biol. 11*, 82–88.
8. Eckert, D. M., and Kim, P. S. (2001) Mechanisms of viral membrane fusion and its inhibition. *Annu. Rev. Biochem. 70*, 777–810.
9. Petka, W. A., Harden, J. L., McGrath, K. P., Wirtz, D., and Tirrell, D. A. (1998) Reversible hydrogels from self-assembling artificial proteins. *Science 281*, 389–392.
10. Muller, K. M., Arndt, K. M., and Alber, T. (2000) Protein fusions to coiled-coil domains. *Methods Enzymol. 328*, 261–282.
11. Chao, H., Bautista, D. L., Litowski, J., Irvin, R. T., and Hodges, R. S. (1998) Use of a heterodimeric coiled-coil system for biosensor

application and affinity purification. *J. Chromatogr. B Biomed. Sci. Appl. 715*, 307–329.
12. Kohn, W. D., and Hodges, R. S. (1998) De novo design of α-helical coiled coils and bundles: models for the development of protein design principles. *Trends Biotechnol. 16*, 379–389.
13. Wang, C., Stewart, R. J., and Kopecek, J. (1999) Hybrid hydrogels assembled from synthetic polymers and coiled-coil protein domains. *Nature 397*, 417–420.
14. Oakley, M. G., and Hollenbeck, J. J. (2001) The design of antiparallel coiled coils. *Curr. Opin. Struct. Biol. 11*, 450–457.
15. Walshaw, J., and Woolfson, D. N. (2001) Socket: a program for identifying and analysing coiled-coil motifs within protein structures. *J. Mol. Biol. 307*, 1427–1450.
16. Maesaki, R., Ihara, K., Shimizu, T., Kuroda, S., Kaibuchi, K., and Hakoshima, T. (1999) The structural basis of Rho effector recognition revealed by the crystal structure of human RhoA complexed with the effector domain of PKN/PRK1. *Mol. Cell 4*, 793–803.
17. Uhlin, U., Cox, G. B., and Guss, J. M. (1997) Crystal structure of the epsilon subunit of the proton-translocating ATP synthase from Escherichia coli. *Structure 5*, 1219–1230.
18. Martin, J., Gruber, M., and Lupas, A. N. (2004) Coiled coils meet the chaperone world. *Trends. Biochem. Sci. 29*, 455–458.
19. Vassylyeva, M. N., Svetlov, V., Dearborn, A. D., Klyuyev, S., Artsimovitch, I., and Vassylyev, D. G. (2007) The carboxy-terminal coiled-coil of the RNA polymerase β' subunit is the main binding site for Gre factors. *EMBO Rep. 8*, 1038–1043.
20. Young, B. A., Anthony, L. C., Gruber, T. M., Arthur, T. M., Heyduk, E., Lu, C. Z., Sharp, M. M., Heyduk, T., Burgess, R. R., and Gross, C. A. (2001) A coiled-coil from the RNA polymerase β'subunit allosterically induces selective nontemplate strand binding by σ^{70}. *Cell 105*, 935–944.
21. Biou, V., Yaremchuk, A., Tukalo, M., and Cusack, S. (1994) The 2.9 Å crystal structure of T. thermophilus seryl-tRNA synthetase complexed with tRNA(Ser). *Science 263*, 1404–1410.
22. Cahuzac, B., Berthonneau, E., Birlirakis, N., Guittet, E., and Mirande, M. (2000) A recurrent RNA-binding domain is appended to eukaryotic aminoacyl-tRNA synthetases. *EMBO J. 19*, 445–452.
23. Borel, F., Vincent, C., Leberman, R., and Hartlein, M. (1994) Seryl-tRNA synthetase from Escherichia coli: implication of its N-terminal domain in aminoacylation activity and specificity. *Nucleic Acids Res. 22*, 2963–2969.
24. Li, Y., Korolev, S., and Waksman, G. (1998) Crystal structures of open and closed forms of binary and ternary complexes of the large fragment of Thermus aquaticus DNA polymerase I: structural basis for nucleotide incorporation. *EMBO J. 17*, 7514–7525.
25. Himeno, H., Hasegawa, T., Ueda, T., Watanabe, K., and Shimizu, M. (1990) Conversion of aminoacylation specificity from tRNA(Tyr) to tRNA(Ser) in vitro. *Nucleic Acids Res. 18*, 6815–6819.
26. Normanly, J., Ollick, T., and Abelson, J. (1992) Eight base changes are sufficient to convert a leucine-inserting tRNA into a serine-inserting tRNA. *Proc. Natl. Acad. Sci. U.S.A. 89*, 5680–5684.
27. Sampson, J. R., and Saks, M. E. (1993) Contributions of discrete tRNA(Ser) domains to aminoacylation by E.coli seryl-tRNA synthetase: a kinetic analysis using model RNA substrates. *Nucleic Acids Res. 21*, 4467–4475.
28. Watanabe, G., Saito, Y., Madaule, P., Ishizaki, T., Fujisawa, K., Morii, N., Mukai, H., Ono, Y., Kakizuka, A., and Narumiya, S. (1996) Protein kinase N (PKN) and PKN-related protein rhophilin as targets of small GTPase Rho. *Science 271*, 645–648.
29. Amano, M., Mukai, H., Ono, Y., Chihara, K., Matsui, T., Hamajima, Y., Okawa, K., Iwamatsu, A., and Kaibuchi, K. (1996) Identification of a putative target for Rho as the serine-threonine kinase protein kinase N. *Science 271*, 648–650.
30. Blumenstein, L., and Ahmadian, M. R. (2004) Models of the cooperative mechanism for Rho effector recognition: implications for RhoA-mediated effector activation. *J. Biol. Chem. 279*, 53419–53426.
31. Owen, D., Lowe, P. N., Nietlispach, D., Brosnan, C. E., Chirgadze, D. Y., Parker, P. J., Blundell, T. L., and Mott, H. R. (2003) Molecular dissection of the interaction between the small G proteins Rac1 and RhoA and protein kinase C-related kinase 1 (PRK1). *J. Biol. Chem. 278*, 50578–50587.
32. Shibata, H., Mukai, H., Inagaki, Y., Homma, Y., Kimura, K., Kaibuchi, K., Narumiya, S., and Ono, Y. (1996) Characterization of the interaction between RhoA and the amino-terminal region of PKN. *FEBS Lett. 385*, 221–224.
33. Flynn, P., Mellor, H., Palmer, R., Panayotou, G., and Parker, P. J. (1998) Multiple interactions of PRK1 with RhoA. Functional assignment of the Hr1 repeat motif. *J. Biol. Chem. 273*, 2698–2705.
34. Modha, R., Campbell, L. J., Nietlispach, D., Buhecha, H. R., Owen, D., and Mott, H. R. (2008) The Rac1 polybasic region is required for interaction with its effector PRK1. *J. Biol. Chem. 283*, 1492–1500.
35. Lu, Y., and Settleman, J. (1999) The Drosophila Pkn protein kinase is a Rho/Rac effector target required for dorsal closure during embryogenesis. *Genes Dev. 13*, 1168–1180.
36. Vincent, S., and Settleman, J. (1997) The PRK2 kinase is a potential effector target of both Rho and Rac GTPases and regulates Actin cytoskeletal organization. *Mol. Cell. Biol. 17*, 2247–2256.
37. Burridge, K., and Wennerberg, K. (2004) Rho and Rac take center stage. *Cell 116*, 167–179.
38. Mukai, H. (2003) The structure and function of PKN, a protein kinase having a catalytic domain homologous to that of PKC. *J. Biochem. (Tokyo) 133*, 17–27.
39. Wei, Y., Zhang, Y., Derewenda, U., Liu, X., Minor, W., Nakamoto, R. K., Somlyo, A. V., Somlyo, A. P., and Derewenda, Z. S. (1997) Crystal structure of RhoA-GDP and its functional implications. *Nat. Struct. Biol. 4*, 699–703.
40. Ihara, K., Muraguchi, S., Kato, M., Shimizu, T., Shirakawa, M., Kuroda, S., Kaibuchi, K., and Hakoshima, T. (1998) Crystal structure of human RhoA in a dominantly active form complexed with a GTP analogue. *J. Biol. Chem. 273*, 9656–9666.
41. Dvorsky, R., and Ahmadian, M. R. (2004) Always look on the bright site of Rho: structural implications for a conserved intermolecular interface. *EMBO Rep. 5*, 1130–1136.
42. Dvorsky, R., Blumenstein, L., Vetter, I. R., and Ahmadian, M. R. (2004) Structural insights into the interaction of ROCKI with the switch regions of RhoA. *J. Biol. Chem. 279*, 7098–7104.
43. Zondlo, N. J., and Schepartz, A. (1999) Highly Specific DNA Recognition by a Designed Miniature Protein. *J. Am. Chem. Soc. 121*, 6938–6939.
44. Montclare, J. K., and Schepartz, A. (2003) Miniature homeodomains: high specificity without an N-terminal arm. *J. Am. Chem. Soc. 125*, 3416–3417.
45. Golemi-Kotra, D., Mahaffy, R., Footer, M. J., Holtzman, J. H., Pollard, T. D., Theriot, J. A., and Schepartz, A. (2004) High affinity, paralog-specific recognition of the Mena EVH1 domain by a miniature protein. *J. Am. Chem. Soc. 126*, 4–5.
46. Chin, J. W., and Schepartz, A. (2001) Concerted evolution of structure and function in a miniature protein. *J. Am. Chem. Soc. 123*, 2929–2930.
47. Chin, J. W., and Schepartz, A. (2001) Design and Evolution of a Miniature Bcl-2 Binding Protein. *Angew. Chem., Int. Ed. 40*, 3806–3809.
48. Gemperli, A. C., Rutledge, S. E., Maranda, A., and Schepartz, A. (2005) Paralog-selective ligands for bcl-2 proteins. *J. Am. Chem. Soc. 127*, 1596–1597.
49. Rutledge, S. E., Volkman, H. M., and Schepartz, A. (2003) Molecular recognition of protein surfaces: high affinity ligands for the CBP KIX domain. *J. Am. Chem. Soc. 125*, 14336–14347.
50. Liu, S., Liu, S., Zhu, X., Liang, H., Cao, A., Chang, Z., and Lai, L. (2007) Nonnatural protein-protein interaction-pair design by key residues grafting. *Proc. Natl. Acad. Sci. U.S.A. 104*, 5330–5335.
51. Sia, S. K., and Kim, P. S. (2003) Protein grafting of an HIV-1-inhibiting epitope. *Proc. Natl. Acad. Sci. U.S.A. 100*, 9756–9761.
52. Domingues, H., Cregut, D., Sebald, W., Oschkinat, H., and Serrano, L. (1999) Rational design of a GCN4-derived mimetic of interleukin-4. *Nat. Struct. Biol. 6*, 652–656.
53. Nygren, P. A., and Uhlen, M. (1997) Scaffolds for engineering novel binding sites in proteins. *Curr. Opin. Struct. Biol. 7*, 463–469.
54. Binz, H. K., and Pluckthun, A. (2005) Engineered proteins as specific binding reagents. *Curr. Opin. Biotechnol. 16*, 459–469.
55. Oakley, M. G., and Kim, P. S. (1997) Protein dissection of the antiparallel coiled coil from Escherichia coli seryl tRNA synthetase. *Biochemistry 36*, 2544–2549.
56. Henaut and Danchin (1996) in *Escherichia coli and Salmonella typhimurium cellular and molecular biology* (Neidhardt, F., Curtiss, R., III, Ingraham, J., Lin, E., Low, B., Magasanik, B., Reznikoff, W., Riley, M., Schaechter, M., and Umbarger, H., Eds.) pp 2047−2066, ASM press, Washington, DC.
57. Ye, Q. Z., Johnson, L. L., and Baragi, V. (1992) Gene synthesis and expression in E. coli for pump, a human matrix metalloproteinase. *Biochem. Biophys. Res. Commun. 186*, 143–149.

58. Chen, G.-Q., Choi, I., Ramachandran, B., and Gouaux, J. E. (1994) Total Gene Synthesis: Novel Single-Step and Convergent Strategies Applied to the Construction of a 779 Base Pair Bacteriorhodopsin Gene. *J. Am. Chem. Soc. 116*, 8799–8800.
59. Prodromou, C., and Pearl, L. H. (1992) Recursive PCR: a novel technique for total gene synthesis. *Protein Eng. 5*, 827–829.
60. Sandhu, G. S., Aleff, R. A., and Kline, B. C. (1992) Dual asymmetric PCR: one-step construction of synthetic genes. *Biotechniques 12*, 14–16.
61. Pan, W., Ravot, E., Tolle, R., Frank, R., Mosbach, R., Turbachova, I., and Bujard, H. (1999) Vaccine candidate MSP-1 from Plasmodium falciparum: a redesigned 4917 bp polynucleotide enables synthesis and isolation of full-length protein from Escherichia coli and mammalian cells. *Nucleic Acids Res. 27*, 1094–1103.
62. Maesaki, R., Shimizu, T., Ihara, K., Kuroda, S., Kaibuchi, K., and Hakoshima, T. (1999) Biochemical and crystallographic characterization of a Rho effector domain of the protein serine/threonine kinase N in a complex with RhoA. *J. Struct. Biol. 126*, 166–170.
63. Ho, S. N., Hunt, H. D., Horton, R. M., Pullen, J. K., and Pease, L. R. (1989) Site-directed mutagenesis by overlap extension using the polymerase chain reaction. *Gene 77*, 51–59.
64. Sanger, F., and Coulson, A. R. (1975) A rapid method for determining sequences in DNA by primed synthesis with DNA polymerase. *J. Mol. Biol. 94*, 441–448.
65. Studier, F. W., Rosenberg, A. H., Dunn, J. J., and Dubendorff, J. W. (1990) Use of T7 RNA polymerase to direct expression of cloned genes. *Methods Enzymol. 185*, 60–89.
66. Edelhoch, H. (1967) Spectroscopic determination of tryptophan and tyrosine in proteins. *Biochemistry 6*, 1948–1954.
67. Chen, Y. H., Yang, J. T., and Chau, K. H. (1974) Determination of the helix and beta form of proteins in aqueous solution by circular dichroism. *Biochemistry 13*, 3350–3359.
68. Laue, T., Shah, B., Ridgeway; T., and Pelletier, S. (1992) Computer-aided interpretation of analytical sedimentation data for proteins, in *Analytical Ultracentrifugation in Biochemistry and Polymer Science* (Harding, S., Rowe, A., and Horton, H., Eds.) pp 90−125, The Royal Society of Chemistry, Cambridge.
69. Sahai, E., Alberts, A. S., and Treisman, R. (1998) RhoA effector mutants reveal distinct effector pathways for cytoskeletal reorganization, SRF activation and transformation. *EMBO J. 17*, 1350–1361.
70. Jaffe, A. B., and Hall, A. (2005) Rho GTPases: biochemistry and biology. *Annu. Rev. Cell Dev. Biol. 21*, 247–269.
71. Cusack, S., Berthet-Colominas, C., Hartlein, M., Nassar, N., and Leberman, R. (1990) A second class of synthetase structure revealed by x-ray analysis of Escherichia coli seryl-tRNA synthetase at 2.5 Å. *Nature 347*, 249–255.

BI8017448